

# **Important Copyright Notice:**

The provision of this paper in an electronic form in this site is only for scholarly study purposes and any other use of this material is prohibited. What appears here is a near-publication draft of the final paper as appeared in the journal or conference proceedings. This is subject to the copyrights of the publishers. Please observe their copyrights.

# Position Sensing in Brake-By-Wire Callipers Using Resolvers

Reza Hoseinnezhad

**Abstract**—Recent designs for brake-by-wire systems use “resolvers” to provide accurate and continuous measurements for the absolute position and speed of the rotor of the electric actuators in brake callipers (permanent magnet DC motors). Resolvers are absolute-angle transducers that are integrated with estimator modules called “angle tracking observer” and together they provide position and speed measurements. Current designs for angle-tracking observers are unstable in applications with high acceleration and/or speed. In this paper, we introduce a new angle-tracking observer in which a closed-loop linear time-invariant (LTI) observer is integrated with a quadrature encoder. Finite-gain stability of the proposed design and its robustness to three different kinds of parameter variations are proven based on theorems of input–output stability in nonlinear control theory. In our experiments, we examined the performance of our observer and two other methods (a well-known LTI observer and an extended Kalman filter) to estimate the position and speed of a brake-by-wire actuator. The results show that because of the very high speed and acceleration of the actuator in this application, the LTI observer and Kalman filter cannot track the rotor position and diverge. In contrast, with a properly designed open-loop transfer function and selecting a suitable switching threshold, our proposed angle-tracking observer is stable and highly accurate in a brake-by-wire application.

**Index Terms**—Brake-by-wire, drive-by-wire, nonlinear observer, resolver, robust stability.

## I. INTRODUCTION

**B**RAKE-BY-WIRE is a frontier technology that will allow many braking functions to switch to electronic actuation and control. When implemented by an electro-mechanical braking (EMB) system, a brake-by-wire system includes four electric callipers (e-callipers). A schematic diagram of the main components of an e-calliper is shown in Fig. 1.

Once the driver inputs a brake command to the system via a human–machine interface (HMI) (e.g., the brake pedal), four independent brake commands are generated by the electronic control unit (ECU) based on high-level brake functions such as antilock braking system (ABS) or vehicle stability control (VSC). These command signals are sent to the four e-callipers via a communication network. As this network might not be able to properly communicate with the e-callipers due to network faults, HMI sensory data are also directly transmitted to each e-calliper via a separate data bus.

Manuscript received May 20, 2005; revised October 18, 2005. This work was supported in part by the Research Centre for Advanced By-Wire Technology (RABiT) and Pacifica Group Technologies Ltd. Pty. The review of this paper was coordinated by Dr. M. A. Masrur.

The author is with the Faculty of Engineering and Industrial Sciences, Swinburne University of Technology, Hawthorn, Victoria 3122, Australia (e-mail: rhoseinnezhad@swin.edu.au).

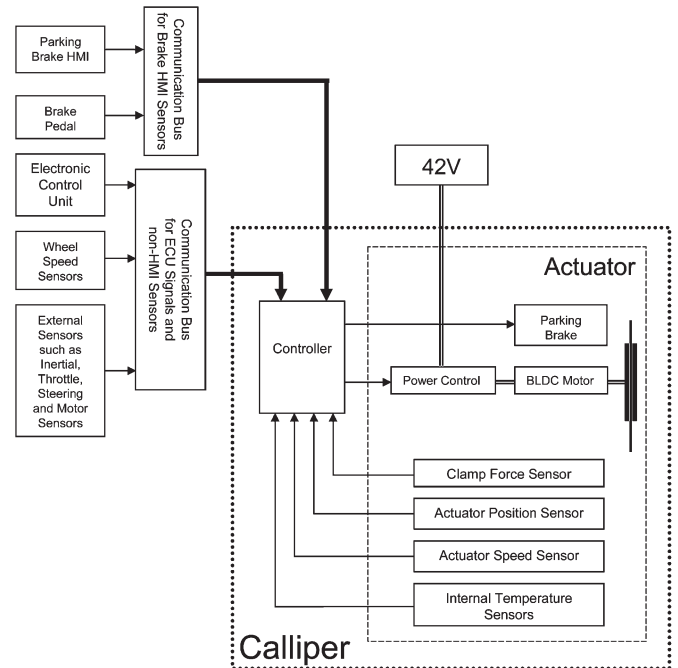


Fig. 1. Schematic diagram of the main components of an e-calliper and their connections to other components in an EMB system.

In each e-calliper, a controller uses the brake command (received from ECU) as a reference input. The controller provides drive control commands for a power control module. This module controls three-phase drive currents for the brake actuator, which is a permanent-magnet DC motor, energized by 42-V sources. In addition to tracking its reference brake command, the calliper controller also controls the position and speed of the brake actuator. Thus, two sensors are vitally required to measure the position and speed of the actuator in each e-calliper. Because of the safety critical nature of the application, even missing a limited number of samples of these sensory data should be compensated for. Hoseinnezhad *et al.* have proposed a new memory efficient method with a low computational overhead to compensate for the missing samples of such vital sensory data [1].

This paper focuses on an efficient design of a measurement mechanism to sense the position and speed of the actuator. Recent designs for brake-by-wire systems use resolvers to provide accurate and continuous measurements for both absolute position and speed of the rotor of the actuators. Incremental encoders are relative position sensors and their additive error needs to be calibrated or compensated for by different methods [2], [3]. Unlike the encoders, resolvers provide two output

signals that always allow the detection of absolute angular position. In addition, they suppress common mode noise and are especially useful in a noisy environment.

A resolver is a rotary transformer with one rotating reference winding (supplied by  $U_{\text{ref}}$ ) and two stator windings. The reference winding is fixed on the rotor and rotates jointly with the shaft passing the output windings. Two stator windings are placed in quadrature of one another and generate the sine and cosine voltages ( $U_{\text{sin}}$  and  $U_{\text{cos}}$ ). The sine winding is phase advanced by  $90^\circ$  with respect to cosine winding. In consequence of the excitement applied on the reference winding and along with the angular movement of the motor shaft  $\Theta$ , the respective voltages are generated by resolver output windings  $U_{\text{sin}}$  and  $U_{\text{cos}}$ . The amplitudes of the generated voltages vary according to the sine and cosine of the shaft angle  $\Theta$ .

Current methods for the estimation of the shaft angle by using the two output signals of the resolver are unstable when they are used for position and speed control of the actuator in an e-calliper. This is mainly due to the nonlinear nature of such estimators and the large extent of controllable speed and acceleration required in this application.

This paper presents a novel design for position and speed estimator that is a stable observer in applications with high speed and acceleration. The proposed method has a demonstrated strong robustness to parameter variations due to manufacturing variation, temperature drifts, and aging. This technique has been patented by the **Research Centre for Advanced By-Wire Technologies (RABiT www.rabit.com.au)** and will be implemented by the industry partner, Pacifica Group Technologies (PGT), for their future brake-by-wire products. In Section II, current methods of position estimation by resolvers are briefly reviewed. Then, the proposed observer is explained, and its stability is mathematically proven in Section III followed by the analysis of its robustness to parameter variations in Section IV. Experimental results are presented in Section V, and Section VI concludes this paper.

## II. RELATED WORK

Resolvers were primarily used in analog design in conjunction with a resolver transmitter–resolver control transformer [4]. These systems were frequently employed in servomechanisms, e.g., in aircraft on-board instrument systems. Modern systems, however, use the digital approach to extract rotor angle and speed from the resolver output signals. The common solution is either a trigonometric or angle-tracking-observer method.

In the trigonometric approach, the shaft angle is determined by an inverse tangent function of the quotient of the sampled resolver output voltages  $U_{\text{sin}}$  and  $U_{\text{cos}}$  given by the following equation:

$$\theta = \text{atan} \left( \frac{U_{\text{sin}}}{U_{\text{cos}}} \right). \quad (1)$$

This approach can be implemented by different DSP chips, e.g., Texas Instruments TMS320F240 [5]. Modern control algorithms for electric drives require knowledge of both the rotor angle and the rotor speed. The trigonometric method, however,

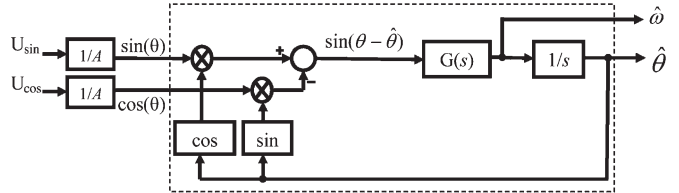


Fig. 2. General systematic diagram of current different designs for ATOs, called as LTI-ATO in this paper.

only yields estimates of the unfiltered rotor angle without any speed information. Therefore, for a final application, a speed calculation with smoothing capability should be added. Furthermore, the four-quadrant inverse tangent results in angles between  $-180^\circ$  and  $180^\circ$ . Thus, the number of turns (required position control) is not tracked.

The above drawbacks are eliminated if an angle-tracking observer (ATO) is utilized [6]. To authors' knowledge, a few different ATO designs have been developed and presented in literature for different applications up to the present. Fig. 2 shows the common systematic diagram of an ATO. In this scheme, the resolver output signals are compared with their corresponding estimates  $\hat{U}_{\text{sin}}$  and  $\hat{U}_{\text{cos}}$ . The Motorola design [7] uses a DSP56F80x to implement this ATO with the following transfer function selected for  $G(s)$  in Fig. 2:

$$G(s) = K_1(K_2 + 1/s). \quad (2)$$

In other attempts, observers with the same tracking scheme shown in Fig. 2 but different transfer functions for  $G(s)$  have been derived. For example, in Harnefors's design, an extended Kalman filter is utilized for speed estimation [8]. In Ellis and Krah's design, a Luenberger observer is applied for angle tracking [9], where in fact the same scheme shown in Fig. 2 resulted with the following open-loop transfer function:

$$G(s)/s = (K_1s^2 + K_2s + K_3)/s^3. \quad (3)$$

Bunte and Beineke have tried to suppress the systematic errors of resolvers with sinusoidal line signals [10]. Benammar *et al.* have proposed a resolver-to-digital converter based on linearization techniques [11]. Kaul *et al.* have utilized look-up tables to improve the accuracy of position estimates given by resolvers [12].

There is, however, a critical issue with the ATO design shown in Fig. 2 and other existing solutions. Although the open-loop observer is linear time-invariant (LTI) (we call it LTI-ATO design henceforward), the closed-loop design is nonlinear (because of the sinusoidal error) and its stability is not guaranteed. Indeed, the tracking error of such an observer will be bounded (converging) only for a limited range of the rate of change of the input signal. Our simulations and experiments have shown that in the case of high rotor speed and/or high acceleration, the LTI-ATO loses its lock to track the angle and speed. In addition, both the trigonometric and the LTI-ATO methods are sensitive to the noise in resolver sinusoidal signals, which exists in industrial applications [13]–[16].

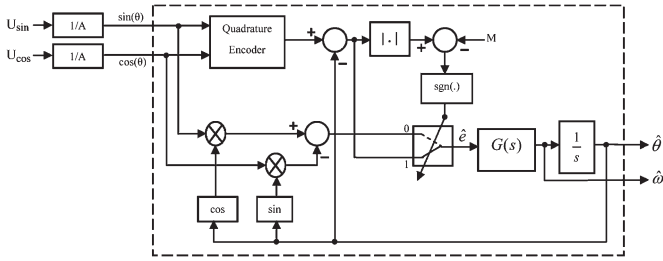


Fig. 3. Block diagram of our proposed ATO.

### III. ATO WITH GUARANTEED STABILITY

In our new design, the LTI-ATO is integrated with a quadrature encoder that tracks the angle with  $90^\circ$  accuracy. It can be easily implemented by two Schmitt triggers that trigger their states at zero crossing points of the  $U_{\sin}$  and  $U_{\cos}$ , respectively, and a counter. The output of such a quadrature encoder, disregarding the noise and the narrow hysteresis band of the Schmitt triggers, is expressed by the following function of the rotor angle:

$$\theta_{\text{quad}} = \frac{\pi}{2} N_{\text{quad}} = \frac{\pi}{2} \left[ \left( \theta + \frac{\pi}{4} \right) / \frac{\pi}{2} \right] \quad (4)$$

where  $[\cdot]$  means “rounding to the nearest integer towards minus infinity.” Due to its discrete nature, the output of the quadrature encoder is robust both to the noise added to the resolver sinusoidal outputs and the hysteresis band of the Schmitt triggers.

The block diagram of our proposed ATO is shown in Fig. 3. The symbol  $|\cdot|$  means “absolute value” and  $\text{sgn}(\cdot)$  is zero or one for negative or nonnegative arguments, respectively.  $M$  is a constant switching threshold. The input signal to the open-loop observer (i.e.,  $G(s)/s$ ) is an error signal  $\hat{e}(t)$  given by the following equation:

$$\hat{e}(t) = \begin{cases} \sin(\theta(t) - \hat{\theta}(t)) & \text{if } |\theta_{\text{quad}}(t) - \hat{\theta}(t)| < M \\ \theta_{\text{quad}}(t) - \hat{\theta}(t) & \text{otherwise} \end{cases} \quad (5)$$

where  $\theta_{\text{quad}}$  is the output of the quadrature encoder.

The absolute position and speed of the rotor are the outputs of a closed-loop observer. The error signal that is fed back to the input of the feed-forward path is initially similar to the feedback error signal in an LTI-ATO design. However, if the observer shows its tendency to diverge, this error signal is switched to another signal, which is the difference between the output angle estimate and the quadrature encoder output. This difference is continually calculated by the ATO, and the switching is carried out if the absolute value of this difference is greater than the threshold  $M$  (alarming that the observer is tending toward divergence).

Before we demonstrate the stability of the proposed closed-loop observer, some preliminary definitions and lemmas from the theory of input–output stability are briefly reviewed as follows.

**Definition 1:** A system is finite-gain stable if there is a constant positive gain  $\gamma$  such that

$$\|y_\tau\| \leq \gamma \|u_\tau\| \quad \text{for all } \tau \quad (6)$$

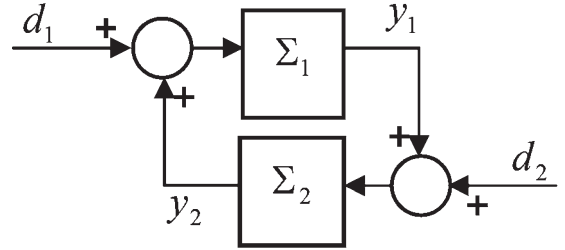


Fig. 4. Standard feedback configuration in the theory of input–output stability.

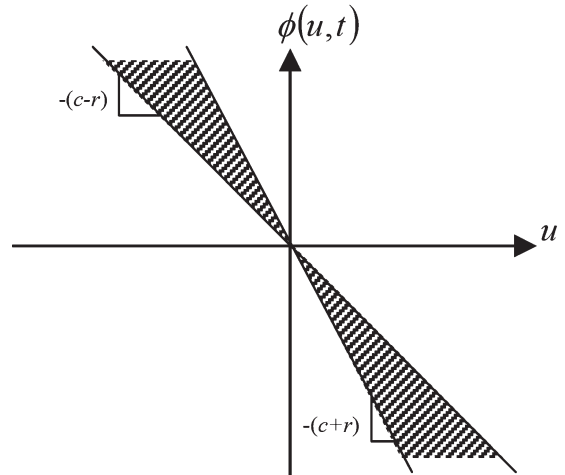


Fig. 5. Graph of  $\text{SECTOR}[-(c+r), -(c-r)]$ .

where  $u(t)$  and  $y(t)$  are the input and output (scalar or vector) signals of the system, respectively,  $\|\cdot\|$  is a norm function (e.g., two-norm or  $\infty$ -norm), and  $u_\tau$  denotes the truncated signal defined as  $u(t)$  in  $[0, \tau]$  and zero in  $(\tau, \infty)$  [17].

The finite-gain stability of a system guarantees its output convergence with limited tracking error. There are different methods to investigate the finite-gain stability of a closed-loop system, including the methods based on small-gain [18], passivity [19], and circle [18]–[22] theorems. Input–output stability-analysis methods are usually expressed and formulated for the standard feedback configuration (shown in Fig. 4).

**Definition 2:** A nonlinearity with input  $u$  and output  $\varphi(u, t)$  belongs to  $\text{SECTOR}[-(c+r), -(c-r)]$  if its graph (its output plotted versus its input) falls inside the shaded area in Fig. 5 ( $c > r > 0$ ) [17], [18].

**Theorem 1 (Circle Theorem):** Consider a closed-loop system with the standard feedback configuration shown in Fig. 4. Assume that  $\Sigma_2$  is a single-input single-output (SISO) system having a real rational transfer function  $G_O(s)$ , and  $\Sigma_1$  is a nonlinearity that belongs to  $\text{SECTOR}[-(c+r), -(c-r)]$  with  $r < c$ . Let  $D_{c,r}$  denote the circular disk in the complex plane centered on the real axis and passing through the points on the real axis with real parts  $-1/(c+r)$  and  $-1/(c-r)$ . The closed-loop system is finite-gain stable if the Nyquist plot of  $G_O(s)$  (with Nyquist path indented into the right-half plane) is outside of and bounded away from the disk  $D_{c,r}$ , and the number of times the plot encircles this disk in the counterclockwise direction is equal to the number of poles of  $G_O(s)$  with strictly positive real parts.

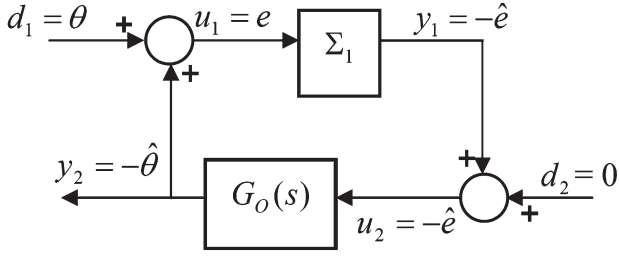


Fig. 6. Block diagram of our proposed ATO redrawn in the form of a standard feedback configuration ( $G_O(s) = G(s)/s$ ).

*Proof:* Refer to [18, Ch. 6, Sec. VI-H] or Sandberg’s papers [20]–[22].

In Fig. 6, we have redrawn our proposed closed-loop ATO in the form of the standard feedback configuration. The transfer function  $G_O(s)$  stands for the open-loop observer, i.e.,  $G(s)/s$  in Fig. 3.  $\Sigma_1$  is a nonlinearity, in which its input is the error signal  $e(t) = \theta(t) - \hat{\theta}(t)$ . Using (5), the output of the nonlinearity  $-\hat{e}(t)$  is the following nonlinear function of its input:

$$-\hat{e}(t) = \begin{cases} -\sin(e(t)) & \text{if } |e(t) + \theta_{\text{quad}}(t) - \theta(t)| < M \\ -(e(t) + \theta_{\text{quad}}(t) - \theta(t)) & \text{otherwise.} \end{cases} \quad (7)$$

**Theorem 2:** The closed-loop ATO design shown in Fig. 3 is finite-gain stable if the following two conditions (called Circle-C3 conditions, henceforward) are met.

- 1) The Nyquist plot of  $G_O(s)$  (with Nyquist path indented into the right-half plane) is outside of and bounded away from the circular disk  $D_{c,r}$  with  $-1/(c+r) = -(M - \pi/4)/M$  and  $-1/(c-r) = -(M + \pi/4)/\sin(M + \pi/4)$ . This disk is denoted by  $D_M$ .
- 2) The number of times the plot encircles  $D_M$  in the counterclockwise direction should be equal to the number of poles of  $G_O(s)$  with strictly positive real parts.

*Proof:* Fig. 7 shows the graph of  $\Sigma_1$ . The term  $\theta_{\text{quad}}(t) - \theta(t)$  in (7) is the quadrature encoder error. Due to this term, the graph of  $\Sigma_1$  includes a shaded area. Fig. 7 shows that in our closed-loop observer,  $\Sigma_1$  belongs to  $\text{SECTOR}[-(c+r), -(c-r)]$  as defined in Definition 2, with the following parameter values:

$$c+r = \frac{M}{M - \frac{\pi}{4}}; \quad c-r = \frac{\sin(M + \frac{\pi}{4})}{M + \frac{\pi}{4}}. \quad (8)$$

Based on (8), circle theorem, and the assumptions given in this theorem, the sufficient conditions for finite-gain stability of the closed-loop system are met. Hence, the system is finite-gain stable.  $\blacksquare$

#### IV. ROBUSTNESS TO PARAMETER VARIATIONS

In this section, two types of parameter variations are studied for their impact on the stability of our closed-loop ATO. The first type of variation is due to environmental noise and temperature drifts. The second type is due to manufacturing variations.

Amplitude and phase-shift variations are two examples in this category of parameter variation that are focused in this section. In the following three sections, we show that variations do not affect the stability of the closed-loop observer if the stability conditions given in Theorem 2 are still met but for a larger disk in the complex plane.

##### A. Noise and Temperature Drifts

In the schematic diagram of our new ATO design in Fig. 3, the resolver output signals  $U_{\sin}$  and  $U_{\cos}$  are assumed to be zero-mean signals. Indeed, the constant predetermined mean (i.e., DC part) of the signals is supposed to be removed before  $U_{\sin}$  and  $U_{\cos}$  are used for angle tracking. In practice, the DC part or the average of the signals provided by the resolvers is not constant, and some variations due to environmental noise and/or temperature drifts apply to these signals.

Assume that the input signals of the ATO design shown in Fig. 3 are given by

$$U_{\sin} = A \sin(\theta) + n_1; \quad U_{\cos} = A \cos(\theta) + n_2 \quad (9)$$

where  $n_1$  and  $n_2$  are the noise and/or temperature drifts and their magnitude fall within  $[-\sigma_n, \sigma_n]$ . As the proposed hybrid estimator uses both the error given by the quadrature encoder and the sine error signal [i.e.,  $\sin(\theta - \hat{\theta})$ ] to avoid divergence, the effect of the noise/drift on both error signals should be studied. Due to this noise/drift, the zero crossing points of  $U_{\sin}$  and  $U_{\cos}$  will shift randomly. This will induce the same shift in the output of the quadrature encoder. Mathematically, (4) should be modified to the following equation

$$\theta_{\text{quad}} = \frac{\pi}{2} \left[ \left( \theta + \frac{\pi}{4} + n_{\theta} \right) / \frac{\pi}{2} \right] \quad (10)$$

where  $n_{\theta}$  is the noise that appears in the quadrature encoder output and is bounded within  $[-\sin^{-1}(\sigma_n/A), \sin^{-1}(\sigma_n/A)]$ .

We remind that the shaded area in the graph of  $\Sigma_1$  (shown in Fig. 7) is the result of the term “ $\theta_{\text{quad}}(t) - \theta(t)$ ” existing in (7), which varies within  $[-\pi/4, \pi/4]$ . This term causes the shaded area between the two boundary lines:  $\hat{e} = e \pm \pi/4$ . In the presence of noise/drift, this term is changed to

$$\theta_{\text{quad}} - \theta = \left\{ \frac{\pi}{2} \left[ \left( \theta + n_{\theta} + \frac{\pi}{4} \right) / \frac{\pi}{2} \right] - (\theta + n_{\theta}) \right\} + n_{\theta}. \quad (11)$$

The first part of the right side of (12) is bounded within  $[-\pi/4, \pi/4]$ , and  $\theta_{\text{quad}}(t) - \theta(t)$  falls within the interval  $[-\pi/4 - \sin^{-1}(\sigma_n/A), \pi/4 + \sin^{-1}(\sigma_n/A)]$ . In other words, the two boundary lines of the shaded area in Fig. 7 change to the following lines:

$$\hat{e} = e \pm (\pi/4 + \sin^{-1}(\sigma_n/A)). \quad (12)$$

Hence, the slope of the upper dotted line (sector boundary in the circle theorem) is

$$c+r = \frac{M}{M - \pi/4 - \sin^{-1}(\sigma_n/A)}. \quad (13)$$

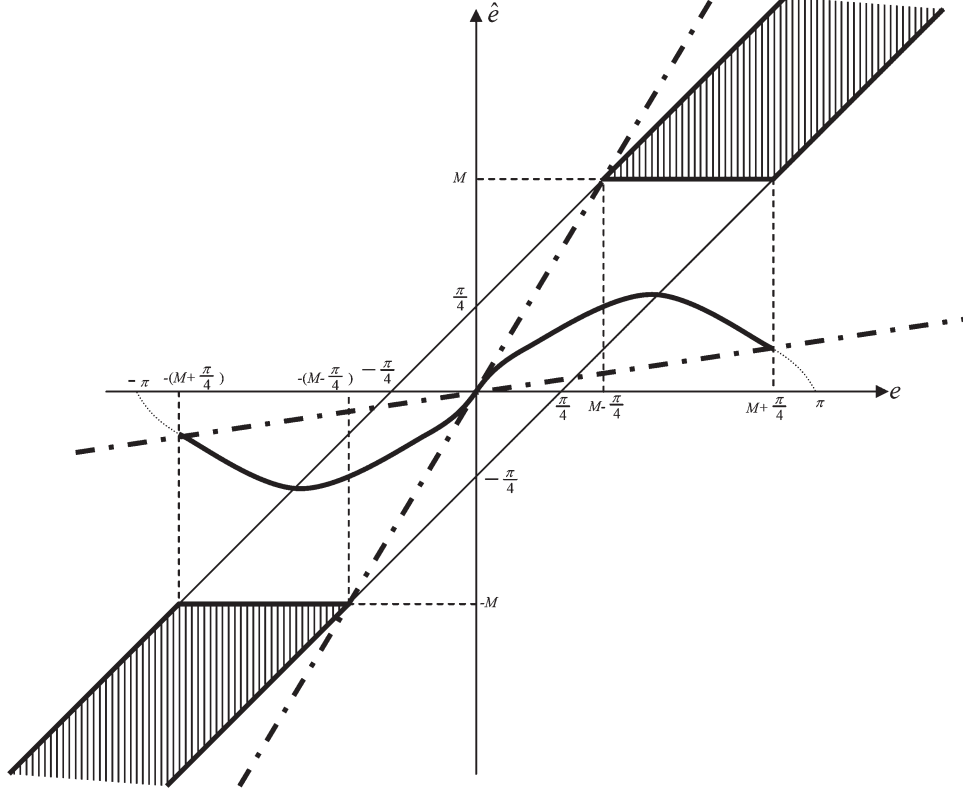


Fig. 7. Graph of the nonlinearity  $-\Sigma_1$  (the solid black sinusoidal curve and the shaded area): Since  $\hat{e}(t)$  has been plotted versus  $e(t)$  and the output of  $\Sigma_1$  is  $-\hat{e}(t)$ , the actual graph of  $\Sigma_1$  can be easily derived by reflecting the above graph with respect to the horizontal axis. The two dotted lines indicate the conic sector to which the graph belongs.

On the other hand, in the presence of noise/drift, the sine error signal calculated by the product-subtract blocks in Fig. 3 is given by the following equation:

$$\begin{aligned} & \frac{U_{\sin}}{A} \cos(\hat{\theta}) - \frac{U_{\cos}}{A} \sin(\hat{\theta}) \\ &= \sin(\theta - \hat{\theta}) + \left\{ \frac{n_1}{A} \cos(\hat{\theta}) - \frac{n_2}{A} \sin(\hat{\theta}) \right\}. \end{aligned} \quad (14)$$

The second term in the right-hand side of the above equation varies between  $-\sqrt{2}\sigma_n/A$  and  $\sqrt{2}\sigma_n/A$ . Considering this variation in the graph of  $\Sigma_1$  (in the sinusoidal section), the slope of the lower dotted line (sector boundary) is given as follows

$$c - r = \frac{\sin(M + \pi/4 + \sin^{-1}(\sigma_n/A)) - \frac{\sqrt{2}\sigma_n}{A}}{M + \pi/4 + \sin^{-1}(\sigma_n/A)}. \quad (15)$$

Based on the circle theorem and the above equations, the closed-loop observer is finite-gain stable if the Circle-C3 conditions are met for the circular disk in the complex plane centered on the real axis and passing through the points on the real axis with real parts given by

$$-(c+r)^{-1} = -[M - \pi/4 - \sin^{-1}(\sigma_n/A)]/M \quad (16)$$

and

$$-(c-r)^{-1} = -\frac{M + \pi/4 + \sin^{-1}(\sigma_n/A)}{\sin(M + \pi/4 + \sin^{-1}(\sigma_n/A)) - \frac{\sqrt{2}\sigma_n}{A}}. \quad (17)$$

## B. Gain Variations

In the proposed method sketched in Fig. 3, the gain of the sine and cosine windings is assumed to be previously known as  $A$ . During mass production, these two amplitudes may slightly vary due to manufacturing variations. Let us assume that the resolver outputs are given by

$$U_{\sin} = (A + \delta_1) \sin(\theta); \quad U_{\cos} = (A + \delta_2) \cos(\theta) \quad (18)$$

where  $\delta_1$  and  $\delta_2$  can vary in  $[-\delta_m, \delta_m]$ . As the zero-crossing points of these signals do not move by amplitude variations, the output of the quadrature encoder does not change. The sine error signal, however, changes as follows

$$\begin{aligned} & \frac{U_{\sin}}{A} \cos(\hat{\theta}) - \frac{U_{\cos}}{A} \sin(\hat{\theta}) \\ &= \left(1 + \frac{\delta_1 + \delta_2}{2A}\right) \sin(\theta - \hat{\theta}) + \frac{\delta_1 - \delta_2}{2A} \sin(\theta + \hat{\theta}). \end{aligned} \quad (19)$$

The term  $|\delta_1 - \delta_2|/2A$  denotes the effect of manufacturing asymmetry between the two windings, and the term  $|\delta_1 + \delta_2|/2A$  denotes the manufacturing variation from one transducer to the other. Since in practice, the latter variation is larger than the former, we assume that  $|\delta_1 - \delta_2| \ll |\delta_1 + \delta_2|$ . Thus,  $\delta_1$  and  $\delta_2$  in (19) are both denoted by  $\delta$ , which varies in  $[-\delta_m, \delta_m]$ .

Again, we focus on the graph of  $\Sigma_1$  (shown in Fig. 7). The dashed area, which corresponds to the output of the quadrature encoder, does not change. For the sinusoidal part of the graph, by substituting  $\delta_1 = \delta_2 = \delta$  in (19), we have

$$\frac{U_{\sin}}{A} \cos(\hat{\theta}) - \frac{U_{\cos}}{A} \sin(\hat{\theta}) = \left(1 + \frac{\delta}{A}\right) \sin(\theta - \hat{\theta}). \quad (20)$$

Thus, the sinusoidal curve is scaled by a factor between  $1 - \delta_m$  and  $1 + \delta_m$ .

The upper dashed (or sector) line in Fig. 7 does not change and  $c + r$  is the same as given by (8). However, the lower dashed line should cover all variations of the sinusoidal curve (including its lower bound). Hence, its gradient is as follows

$$c - r = \frac{\left(1 - \frac{\delta_m}{A}\right) \sin(M + \pi/4)}{M + \pi/4}. \quad (21)$$

Based on circle theorem and the values of  $c - r$  and  $c + r$  given by (21) and (8), the closed-loop observer is finite-gain stable if the Circle-C3 conditions are met for the circular disk  $D_{c,r}$  with

$$-(c + r)^{-1} = -(M - \pi/4)/M \quad (22)$$

and

$$-(c - r)^{-1} = -(M + \pi/4)/[(1 - \delta_m/A) \sin(M + \pi/4)]. \quad (23)$$

### C. Phase-Shift Variations

In the resolver, the sine winding should be phase advanced by exactly  $90^\circ$  with respect to the cosine winding. Due to two main reasons, this phase shift can deviate from  $90^\circ$ : aging (gradual shift) and manufacturing misalignments (initial constant shift). Let the phases of the sine and cosine signals are shifted by  $\Delta_1$  and  $\Delta_2$ , and the resolver signals are given by

$$U_{\sin} = A \sin(\theta + \Delta_1); \quad U_{\cos} = A \cos(\theta + \Delta_2) \quad (24)$$

where  $-\Delta_m \leq \Delta_i \leq \Delta_m$ ,  $i = 1, 2$ , and  $\Delta_m$  is a small angle. The effect of the phase shifts on both the error given by the quadrature encoder and the sine error signals are studied. For the first error, (10) and (11) apply again in this case with  $-\Delta_m \leq n_\theta \leq \Delta_m$ . Thus, the two boundary lines of the shaded area in Fig. 7 change to the following lines:

$$\hat{e} = e \pm (\pi/4 + \Delta_m). \quad (25)$$

Thus, the gradient of the upper dashed (or sector) line in Fig. 7 changes to  $c + r = M/(M - \pi/4 - \Delta_m)$ . Since phase deviations are small in practice, we assume that  $\sin(\Delta_i) \approx \tan(\Delta_i) \approx \Delta_i$ ;  $i = 1, 2$ . By this assumption, the sine error signals will be given by the following equation:

$$\begin{aligned} \frac{U_{\sin}}{A} \cos(\hat{\theta}) - \frac{U_{\cos}}{A} \sin(\hat{\theta}) &= \sin(\theta - \hat{\theta}) \\ &+ \frac{\Delta_1 + \Delta_2}{2} \cos(\theta - \hat{\theta}) + \frac{\Delta_1 - \Delta_2}{2} \cos(\theta + \hat{\theta}). \end{aligned} \quad (26)$$

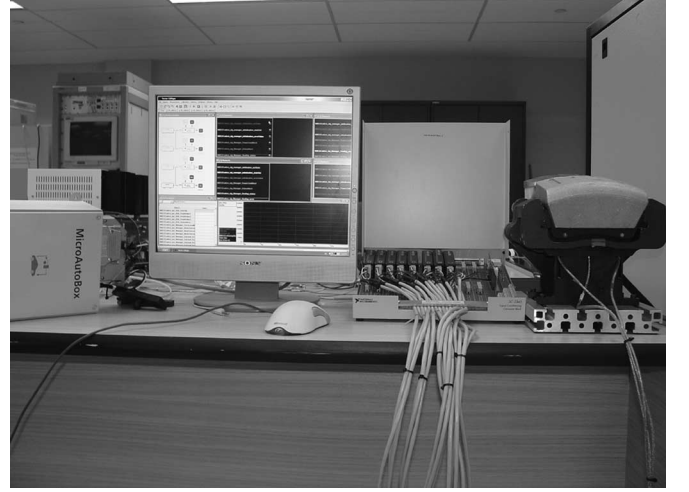


Fig. 8. Our experimental setup using the brake-by-wire designed in Pacifica Group Technologies Ltd. Pty.

It is easy to observe that the deviation of this error signal from  $\sin(\theta - \hat{\theta})$  varies within  $[-2\Delta_m, 2\Delta_m]$ . Consequently, the sinusoidal curve in Fig. 7 will be vertically shifted up or down by no more than  $2\Delta_m$ . Thus, the gradient of the lower dashed (or sector) line in Fig. 7 changes to  $c - r = (\sin(M + \pi/4) - 2\Delta_m)/(M + \pi/4)$ .

Based on circle theorem and the above discussion, the closed loop observer is finite-gain stable if the Circle-C3 conditions are met for the circular disk  $D_{c,r}$  with

$$-(c + r)^{-1} = -\frac{M - \pi/4 - \Delta_m}{M} \quad (27)$$

and

$$-(c - r)^{-1} = -\frac{M + \pi/4}{\sin(M + \pi/4) - 2\Delta_m}. \quad (28)$$

## V. EXPERIMENTAL RESULTS

In order to evaluate the performance of the proposed ATO design in terms of its robust stability and tracking accuracy, we have run a number of experiments using an electro-mechanical braking (EMB) system, which has been recently designed by Pacifica Group Technologies Ltd. Pty. The architecture of the e-calliper and its connections to other components in the EMB system is similar to Fig. 1. However, in our test rig, we added a high-resolution encoder to the system so as to record the true rotor position signal. A photograph of our test rig is shown in Fig. 8, including its two main components: the ECU and the calliper.

The resolver output signals were recorded by two 12-bit analog-to-digital converters. Based on the nominal amplitude of the sine and cosine signals, given by the data sheet of the resolver, the gain  $A$  in Fig. 3 was calculated and set to 920.

A sequence of multiple brake demands was generated in the system by asking the driver to push his foot on the pedal several times (each time harder than the previous one). By

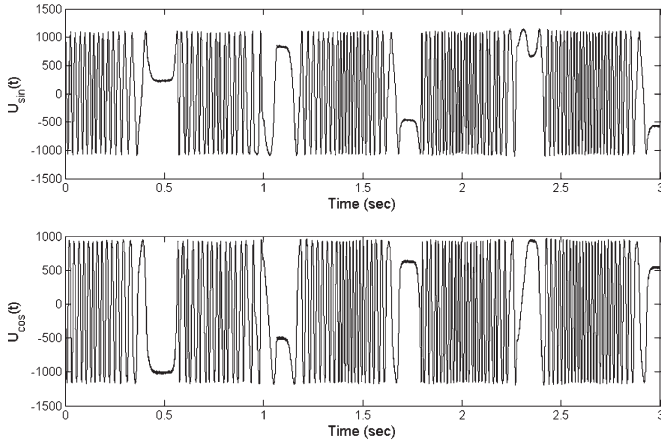


Fig. 9. Resolver signals during the first 3 s of the experiment.

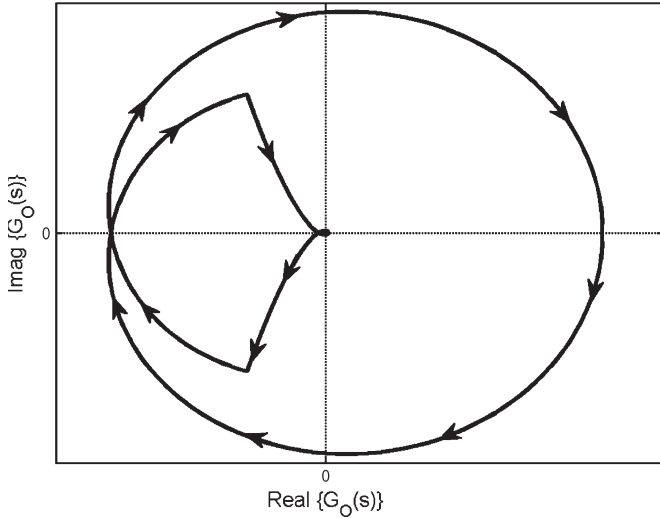


Fig. 10. Complete Nyquist plot of the  $G_O(s)$  given by (29), with the Nyquist path indented into the right-half plane.

using hardware-in-the-loop (HIL) simulation that was run by a vehicle dynamic simulation software, and based on high-level braking functions (ABS and VSC), the ECU generated brake commands for the four callipers in terms of the clamp force that should be generated in each calliper. A local controller in each calliper generated drive currents for the actuator. In addition to the clamp force sensed by the force sensor, these closed-loop controllers also used the position and speed estimates given by our ATO to control the speed of the actuator besides the generated clamp force.

The resolver signals and the true position of the actuator rotor were recorded during 25 s of the trial. Fig. 9 shows the resolver signals during the first 3 s of the experiment. The amplitude analysis of the resolver signals shows that the actual amplitudes of the sine and cosine signals are 1065 ( $\delta_1 = 145$ ) and 1040 ( $\delta_2 = 120$ ), respectively. Since  $|\delta_1 + \delta_2| \gg |\delta_1 - \delta_2|$ , we can use the robust stability criteria given in (22) and (23) with  $\delta_m/A = 145/920 = 0.1576$  and  $M = \pi/2$ , resulting in a circular disk  $D_{c,r}$  with  $-1/(c+r) = -0.5$  and  $-1/(c-r) = -3.9556$ .

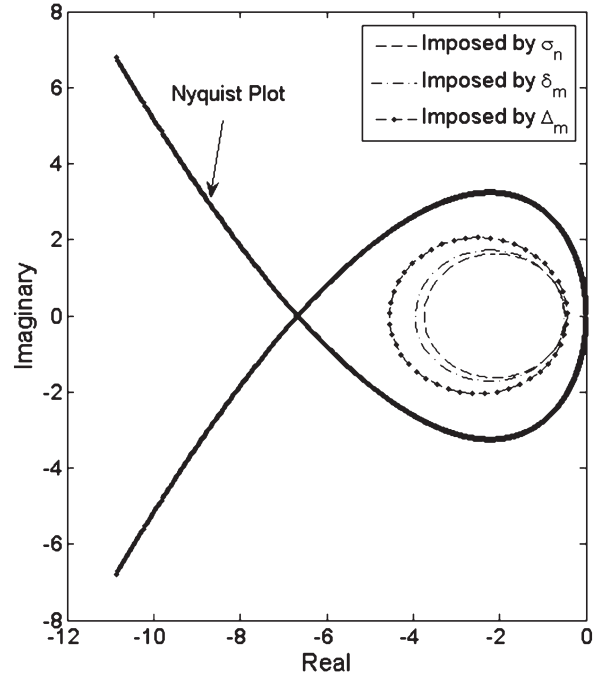


Fig. 11. Nyquist plot shown in Fig. 10, zoomed in around the origin.

The noise analysis of the signals shows a maximum deviation of  $\sigma_n = 30$  in the signals. Equations (16) and (17) result in  $-1/(c+r) = -0.4792$  and  $-1/(c-r) = -3.7467$  for another circular disk  $D_{c,r}$ . Moreover, the actual phase difference between the two signals was calculated as  $84.59^\circ$ . Based on the discussion given in Section IV-C and (27) and (28) with  $\Delta_m = 90 - 84.59 = 5.41^\circ$  and  $M = \pi/2$ , a third circular disk  $D_{c,r}$  is given by  $-1/(c+r) = -0.4399$  and  $-1/(c-r) = -4.5463$ .

For  $M = \pi/2$ , the following open-loop transfer function meets Circle-C3 conditions for the above three circular disks:

$$G_O(s) = G(s)/s = \frac{40s^2 + 150s + 900}{s^3}. \quad (29)$$

Fig. 10 shows the Nyquist plot of  $G_O(s)$  with the Nyquist path indented into the right-half plane. This plot has been zoomed in around the origin and plotted along with the three disks (imposed by  $\delta_m$ ,  $\sigma_n$ , and  $\Delta_m$ ) in Fig. 11. The Nyquist plot encircles these discs once in clockwise direction (as observed in Fig. 10) and once in counterclockwise direction (as shown in Fig. 11). The algebraic sum of turns is zero, which is equal to the number of poles of  $G_O(s)$  with strictly positive real parts. Hence, the ATO should be a stable observer in the presence of all mentioned variations.

Fig. 12 shows the real angular position and its estimates given by an LTI-ATO (as devised in [5]) and an extended Kalman filter (as devised in [8]). This figure demonstrates that both the LTI-ATO and Kalman filter are unstable due to the very high speed and acceleration (particularly after 20 s) and the parameter variations, as discussed before.

The true position of the actuator rotor and the error of the position estimate that is provided by our proposed ATO are shown in Fig. 13. This figure shows that the proposed ATO design is stable and provides an estimate of the position with

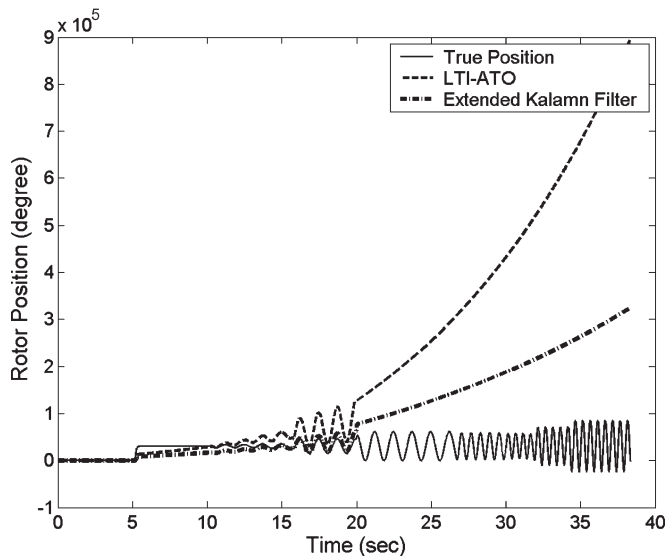


Fig. 12. Real and estimated angle and speed, by the resolver and Kalman filtering methods, in Case 1.

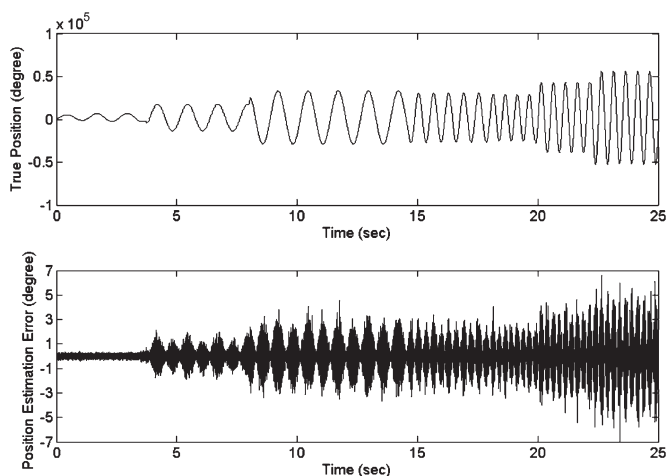


Fig. 13. True position of the actuator rotor (upper) and the error of the position estimated by the proposed ATO (lower).

a tracking error of not more than  $7^\circ$ , which is far less than the maximum error of  $90^\circ$  observed by a quadrature encoder.

## VI. CONCLUSION

A new ATO was introduced in this paper. In this hybrid design, the sinusoidal outputs of a resolver are processed in two different manners. On one side, they are combined with the output feedback of the estimator, providing the sinus of the estimation error. On the other side, their zero crossing points are counted by two Schmitt trigger units in a quadrature encoder, and an estimate for the angular position is provided with maximum error of  $90^\circ$ . The ATO output feedback is also subtracted from this quadrature encoder, giving another estimation error. Depending on the magnitude of this error, either this error signal or the sinus of the estimation error is given to the input of an LTI open-loop observer whose outputs are position and speed estimates.

Finite-gain stability of this ATO design was proven based on circle theorem. Its robustness to three different types of parameter variations that happen in practice was also investigated. Experimental results showed that in the case of high actuator speed and acceleration demanded by a brake-by-wire system, LTI-ATO design and extended Kalman filter are unstable but our ATO design can track the position and speed of the actuator with a maximum error of  $7^\circ$ .

## REFERENCES

- [1] R. Hoseinnezhad and A. Bab-Hadiashar, "Missing data compensation for safety-critical components in a drive-by-wire system," *IEEE Trans. Veh. Technol.*, vol. 54, no. 4, pp. 1304–1311, Jul. 2005.
- [2] R. Hoseinnezhad, M. R. Asharif, and B. Moshiri, "Improved pose estimation for mobile robots by fusion of odometry data and environment map," *J. Intell. Robot. Syst.*, vol. 36, no. 1, pp. 89–108, Jan. 2003.
- [3] M. R. Asharif, B. Moshiri, and R. Hoseinnezhad, "Intelligent mobile robot perception by using a new concept for sensor data fusion: Pseudo information measure," *ISA Trans.*, vol. 41, no. 3, pp. 283–302, Jul. 2002.
- [4] P. Kohl and T. Holomek, "Hollow shaft resolvers—Modern position sensors, ATAS Elektromotory a.s. Nachod," 2000. project report.
- [5] M. Staebler, (2000, Feb.). "TM320F240 DSP solution for obtaining resolver angular position and speed," Texas Instrument Application Rep. SPRA605. [Online]. Available: [www.eetkorea.com/ARTICLES/2001MAY/2001MAY18\\_AMD\\_D\\_SP\\_AN2.PDF](http://www.eetkorea.com/ARTICLES/2001MAY/2001MAY18_AMD_D_SP_AN2.PDF)
- [6] D. Morgan, "Tracking demodulation," *Embedded Syst. Program.*, vol. 14, no. 1, pp. 115–120, Jan. 2001.
- [7] M. Mienkina, P. Pekarek, F. Dobes, (2002). "DSP56F80x resolver, driver and hardware interface," Motorola Inc. Application Rep. AN1942/D. [Online]. Available: [http://www.freescale.com/files/product/doc/AN1942\\_D.pdf](http://www.freescale.com/files/product/doc/AN1942_D.pdf)
- [8] L. Harnefors, "Speed estimation from resolver noisy signals," in *Proc. IEE Conf. Power Electron. Var. Speed Drives*, Sep. 1996, pp. 279–282.
- [9] G. Ellis and J. O. Kraha, "Observer-based resolver conversion in industrial servo systems," in *Proc. PCIM Conf.*, Nuremberg, Germany, 2001, pp. 311–316.
- [10] A. Bunte and S. Beineke, "High-performance speed measurement by suppression of systematic resolver and encoder errors," *IEEE Trans. Ind. Electron.*, vol. 51, no. 1, pp. 49–53, Feb. 2004.
- [11] M. Benammar, L. Ben-Brahim, and M. A. Alhamadi, "Novel resolver-to-360 degrees linearized converter," *IEEE Sens. J.*, vol. 4, no. 1, pp. 96–101, Feb. 2004.
- [12] S. K. Kaul, R. Koul, C. L. Bhat, I. K. Kaul, and A. K. Tickoo, "Use of a 'look-up' table improves the accuracy of a low-cost resolver-based absolute shaft encoder," *Meas. Sci. Technol.*, vol. 8, no. 3, pp. 329–331, Mar. 1997.
- [13] G. Ellis, "Technology update—Observers improve resolver conversion in motion systems," *Control Eng.*, vol. 49, no. 1, pp. 8–11, Jan. 2002.
- [14] C. H. Yim, I. J. Ha, and M. S. Ko, "A resolver-to-digital conversion method for fast tracking," *IEEE Trans. Ind. Electron.*, vol. 39, no. 5, pp. 369–378, Oct. 1992.
- [15] S. Morimoto, K. Kawamoto, and Y. Takeda, "Position and speed sensorless control for IPMSM based on estimation of position error," *Electr. Eng. Jpn.*, vol. 144, no. 2, pp. 43–52, Jul. 2003.
- [16] K. A. Corzine and S. D. Sudhoff, "Hybrid observer for high performance brushless DC motor drives," *IEEE Trans. Energy Convers.*, vol. 11, no. 2, pp. 318–323, Jun. 1996.
- [17] A. R. Teel, T. T. Georgiou, L. Praly, and E. Sontag, "Input-output stability," in *The Control Handbook*, 1st ed. W. S. Levine, Ed. Boca Raton, FL: CRC Press, 1996, pp. 895–908.
- [18] H. J. Marquez, *Nonlinear Control Systems: Analysis and Design*. Hoboken, NJ: Wiley, Apr. 2003, ch. 6.
- [19] H. K. Khalil, *Nonlinear Systems*, 3rd ed. Upper Saddle River, NJ: Prentice-Hall, 2002, ch. 6.
- [20] I. W. Sandberg, "A frequency-domain condition for the stability of feedback systems containing a single time-varying nonlinear element," *Bell Syst. Tech. J.*, vol. 43, no. 4, pp. 1601–1608, Jul. 1964.
- [21] —, "Some results on the theory of physical systems governed by nonlinear functional equations," *Bell Syst. Tech. J.*, vol. 44, no. 5, pp. 871–898, May/June 1965.
- [22] —, "On the L-boundedness of solutions of nonlinear functional equations," *Bell Syst. Tech. J.*, vol. 43, no. 4, pp. 1581–1599, Jul. 1964.



**Reza Hoseinnezhad** was born in Tehran, Iran, in 1973. He received the B.E., M.E., and Ph.D. degrees from the University of Tehran, Iran, in 1994, 1996, and 2002, respectively, all in electrical engineering.

From 2002 to 2003, he was an Assistant Professor at the University of Tehran. From July 2003 to October 2005, he was a Postdoctoral Research Fellow, and since October 2005, he has been a Senior Research Fellow, at Swinburne University of Technology, Victoria, Australia. His research is focused on new methodologies for signal process-

ing and sensor-data-fusion techniques applied in drive-by-wire systems, and on the analysis of robust estimation techniques in computer vision. He has one international and one Australian patents on brake-by-wire systems. His research interests are signal processing, robust estimation, control-system design, and autonomous mobile robotics in general, and sensor data fusion in particular.